SUPPORTING INFORMATION

3D Printing with Waste High-Density Polyethylene

Aniket Gudadhe[1], Nirmalya Bachhar[1], Anil Kumar[2], Prem Andrade[2], Guruswamy Kumaraswamy*[1]

[1]J-101, Polymers and Advanced Materials Laboratory, Complex Fluids and Polymer Engineering, Polymer Science and Engineering, CSIR-National Chemical Laboratory, Pune 411008, Maharashtra, India

[2] ANSYS Software India Pvt. Ltd., Hinjewadi, Phase-1, Pune 411057, Maharashtra, India

Corresponding Author

* Guruswamy Kumaraswamy (Email: g.kumaraswamy@ncl.res.in)

Table S 1. Literature summary of the efforts to FFF print HDPE

Material	Method/Preparation	3D Printing	Results	References
Recycled HDPE from milk jugs	Not described	Large format non-standard FFF printer converted from a plasma cutter. Printed with a sacrificial flange mechanically screwed to build plate. Pegboard with countersunk holes used as print substrate	Specialised print substrate provided a mechanical bond and heaters on the print head melted the layers below for adhesion. In combination with the bolted flange, this solution allowed for printing of a large boat.	3D Printing a Functional Boat with Post-Consumer Milk Jugs 2013[1]
Commercial HDPE reinforced with compatibilized TMP fibers	Compounded using single screw extruder	Standard FFF. No heated print substrate.	Low MFI HDPE grade showed better printability compared to higher grade	Filgueira et al. 2018[2]
HDPE – Core PC/ABS – Shell	Core-shell filament made using two single screw extruders with a co-extrusion die	Standard FFF printer. print substrate heated at 120°C, covered by Kapton tape with thin layer of PVA based glue on top	PC/ABS core with adhesion provided due to heated print substrate covered by Kapton with thin PVA based glue allows for printing without severe warpage	Peng et. al. 2019[3]
Neat commercial virgin HDPE	Filament made using twin-screw extruder and a winding unit	Standard FFF printer. Specialised SEBS block copolymer plate heated at 60°C was used as print substrate	SEBS provided good adhesion throughout print process for printing test specimens	Schirmeister et. al. 2019[4]
Recycled HDPE compounded with Millad 3988i and LLDPE	Filament was made by extruding the compositions through a capillary rheometer and using a home-built wind-up unit to achieve desired	Standard FFF printer. Printing was done on a glass print substrate covered with a thin layer of PVA-based glue with a brim attached to the object	Additives along with print strategy resulted in minimal warpage and allowed for printing of different shaped objects	Our work

	diameter			

S1. Characterization of recycled HDPE

Material:

Waste-derived HDPE: Waste-derived HDPE was received in the form of shredded flakes (washed and dried) from a local waste-collection organization, SWaCH. Sorbitol derivative DMDBS (Trade name: Millad 3988i) was supplied by Milliken, USA. All the materials were used as obtained without further modification. LLDPE grade used was Dowlex 2045G with MFI of 1 g/10min (190°C/2.16kg) manufactured by Dow Chemical Company, USA.

Formulated virgin HDPE: We used Relene HD53EA010 grade of HDPE with melt flow index (MFI) of 1 g/10min (190 ˚C/2.16kg) supplied by Reliance Industries Limited, India. To formulate the virgin HDPE to prepare filaments for FFF, we compounded it with LLDPE and DMDBS in exactly the same manner as for the waste-derived HDPE.

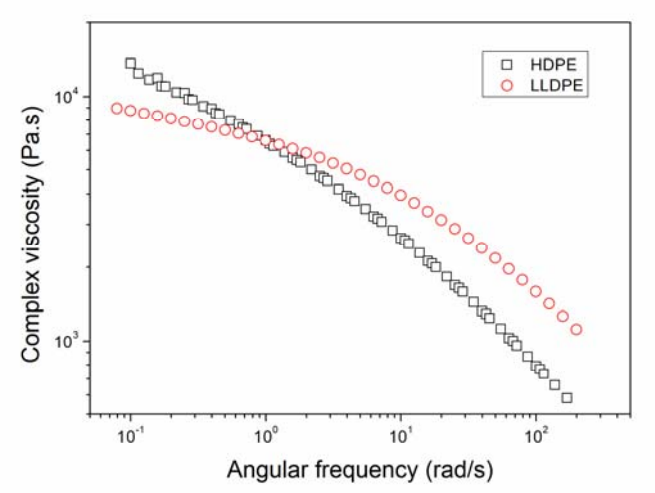

Figure S 1. Comparison between the complex viscosity between waste driven HDPE and LLDPE. The experiments were carried out in ARES G2, TA Instruments, with ω = 0.1 to 100 and 5% strain at 190 ˚C.

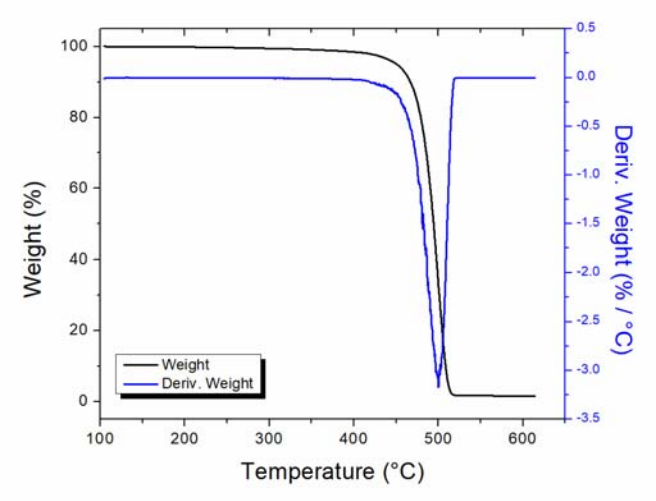

Figure S 2. Thermogravimetric analysis of waste-derived HDPE under N_2 atmosphere showing a single peak in the derivative of TGA weight loss (blue line). The experiments were done in TGA Q5000 of TA instruments with temperature ramp of 20 ˚C per min from 100 ˚C to 700 ˚C. The temperature was initially equilibrated at 100 ˚C for 5 min before the temperature sweep to remove any additional moisture from the sample. The onset of weight decrease (~5% change from the initial plateau) was at 459.7 ˚C and the sample weight plateaus at 500.3 ˚C. The final ash content was found to be about 1%.

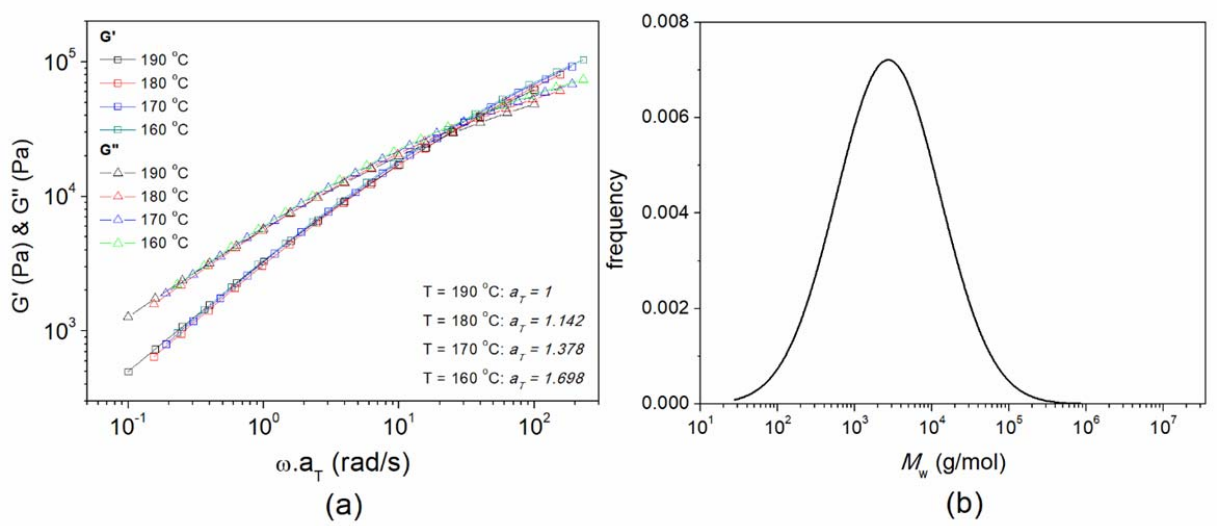

Figure S 3. Time-Temperature superposition (TTS) master curve of waste-derived HDPE is shown in Figure S3(a). Using the TTS master curve, we obtain the molecular weight distribution (Figure S3b) of the polymer using the double reptation mixing rule following Mead[5]. The rheology data (obtained form the ARES G2, TA Instruments, with ω = 0.1 to 100 and 5% strain) is inverted to obtain the MWD using software provided by TA Instruments. The estimated number average molar mass (M_n) is 9004.84 g/mol, mass average molar mass (M_w) is 98986.8 g/mol and the polydispersity index is 10.99.

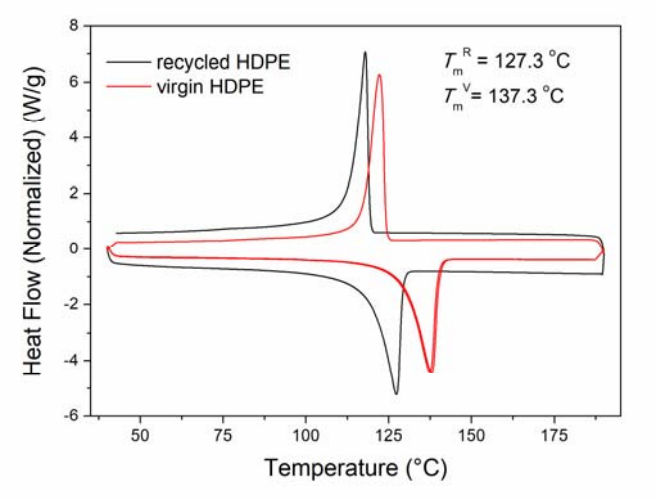

Figure S 4. Differential scanning calorimetry data showing the melting (127.3 ˚C) and crystallization peak (117.9 ˚C) of waste-derived HDPE. The experiments were performed using DSC Q10, TA instruments. The temperature were equilibrated at 190 ˚C for 2 min to remove the thermal history form the sample. The sample was cooled from the melt state (190 ˚C) to room temperature (40 ˚C) at 10 ˚C/min to obtain the crystallization data and was subsequently heated at a rate of 10 ˚C/min to characterize melting behavior.

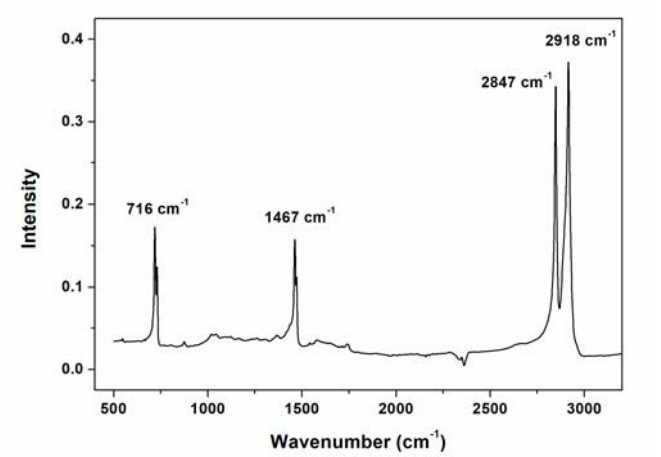

Figure S 5. FT-IR Spectrum of waste-derived HDPE. The measurements are performed on a thin film of HDPE using TENSOR II, Bruker in ATR mode, using a diamond crystal (64 scans, 4 cm^{-1} resolution).

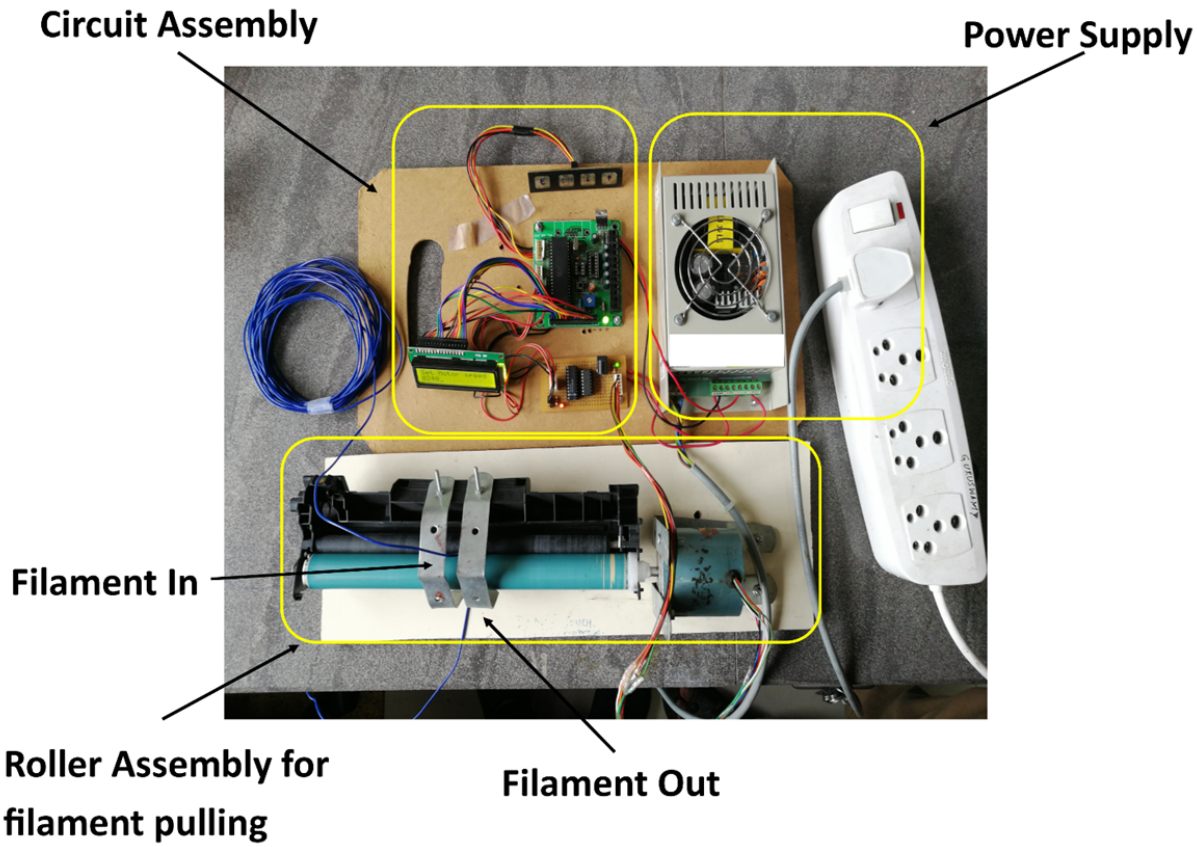

Figure S 6. Home-built wind-up unit for pooling the filament

Details of home-built wind-up unit:

The winding unit consists of a set of rollers that grip and pull the extruding plastic strand with constant speed converting it into a filament with uniform diameter.

Here, we cut open a used printer cartridge, used with a regular laser printer, and salvaged the roller assembly. The cartridge had two types of rollers: a cushioned roller and a hard-top roller. This was ideally suited to our application since the cushioned roller grips the filament well against the hard surface of the other roller. A small stepper motor obtained at a local hardware store was fixed to the cushioned roller with the help Araldite® permanent glue. The motor was controlled by a unit that runs the motor at fixed RPM values. We chose to use a stepper motor in this unit as it maintains a constant motor rpm, even as the load increases due to filament being pulled. The entire assembly of rollers attached with stepper motor was fixed on a wooden platform for stability. The set up was manually optimized and we observed that a motor rpm of 24 yielded a filament with diameter ranging from 1.68mm to 1.72mm.

S2. Image analysis of warped 3D printed object

In order to obtain the accurate warpage of the 3D printed objects, we have scanned a high-resolution (600 dpi) image of individual object laid on their side. Subsequently the images were analyzed by ImageJ software to identify the coordinates of the bottom (shown in Figure S1) and top surfaces. The maximum warpage is observed at the edges and the minimum warpage is observed at the center. We have measured the maximum thickness of the object around the center using a micrometer. The maximum value of the difference between the top and bottom coordinate in mm is termed the warpage (W) and is reported in the Figure 3 of the main manuscript.

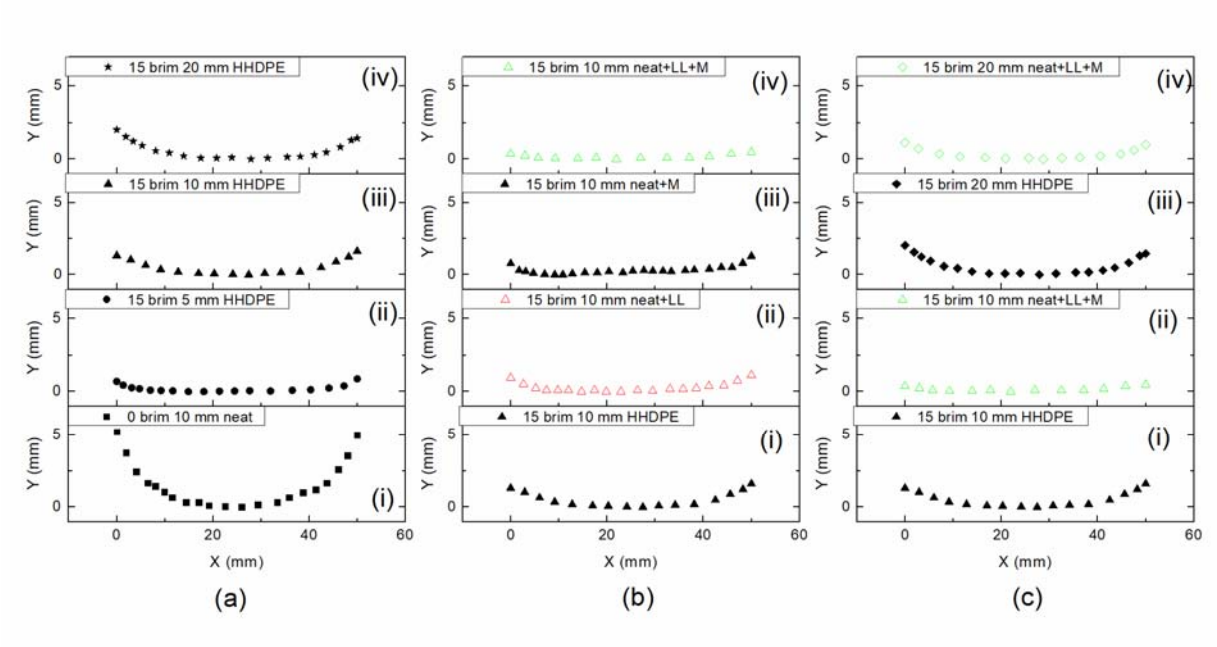

Figure S 7. Warpage profile of different objects obtained using image analysis. All objects are printed with a 15-line brim, except when specified. The left column (a) shows the warpage profiles of waste-derived HDPE bars of different height. (i) 10 mm (tall) object with no brim, (ii) 5 mm (tall) object, (iii) 10 mm (tall) object and (iv) 20 mm (tall) object. The middle column (b) shows the comparison of 10 mm tall objects with different composition. (i) waste-derived HDPE, (ii) 10 wt.% LLDPE blended with waste-derived HDPE, (iii) 0.4 wt.% DMDBS blended with waste-derived HDPE and (iv) 0.4 wt.% DMDBS and 10 wt.% LLDPE blended with waste-derived HDPE. The right column (c) shows the effect of height on the warpage of both (neat) waste-derived HDPE and f-HDPE bars with height = (i) 10 mm waste-derived HDPE, (ii) 10 mm f-HDPE, (iii) 20 mm waste-derived HDPE and (iv) 20 mm f-HDPE.

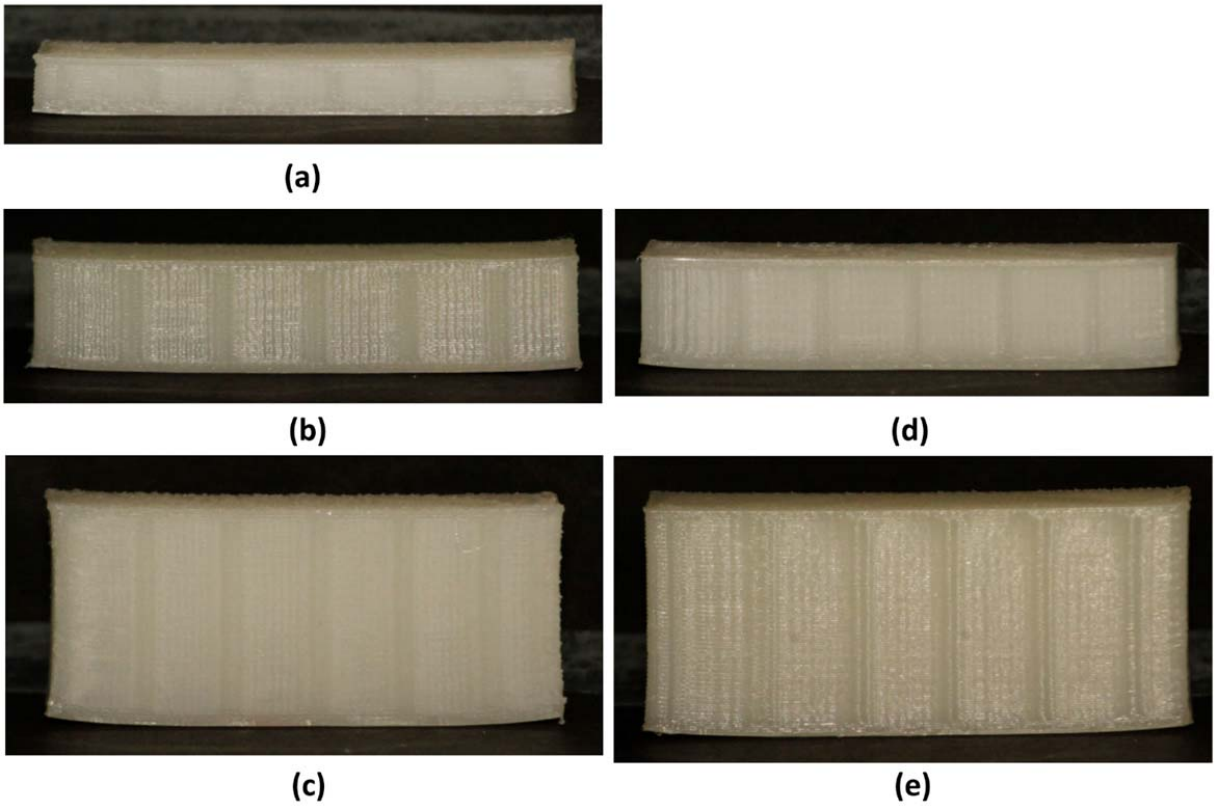

Figure S 8. Effect of bar height on warpage. The left column (a-c) shows FFF printed neat virgin commercial HDPE and the right column (d-e) shows the same for formulated HDPE prepared using the same virgin material, for rectangular bars with different heights. The object heights are: (a) 5 mm, (b) & (d) 10 mm (c) & (e) 20 mm. The warpage comparison of these objects is shown in Figure S3.

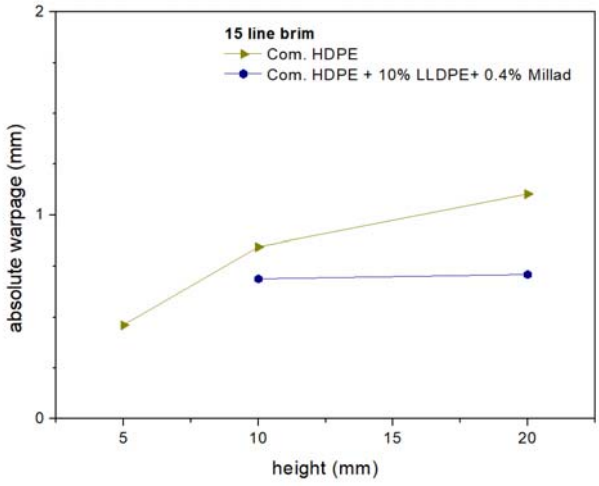

Figure S 9. The warpage comparison between all different samples of commercial HDPE and composition having different height as shown in Figure S3.

Table S 2. Overall dimension of the warped

Object description	Print dimension specified	Print dimension obtained
fHDPE, 13.5 mm brim	50 mm × 15 mm × 10 mm	49.5 mm × 14.6 mm × 10 mm
fHDPE, 13.5 mm brim	50 mm × 15 mm × 20 mm	48.5 mm × 14.5 mm × 20 mm

S3. Mathematical modeling of the warpage of 3D printed HDPE

Here, we present a mathematical model that was employed to qualitatively capture warpage of FFF printed semi-crystalline polymers. The thermo-mechanical model was constructed and solved using ANSYS Workbench Additive software tool. The transient heat conduction equation solved is given by equation S1.[6–8]

$$\frac{\partial}{\partial x}\left(k_x \frac{\partial T}{\partial x}\right) + \frac{\partial}{\partial y}\left(k_y \frac{\partial T}{\partial y}\right) + \frac{\partial}{\partial z}\left(k_z \frac{\partial T}{\partial z}\right) + q = \rho c \frac{\partial T}{\partial t} \qquad \text{(S1)}$$

where, ρ, c, q, T, t are material density, specific heat, heat generation per unit volume, temperature and time, respectively. The thermal conductivities in x, y and z directions are represented as k_x, k_y, k_z respectively. The actual printer head lays one strand of filament and builds up the layer by translating in the XY plane. However, to avoid computationally expensive FE modelling to capture deposition of each individual line of filament, we used a deposition of one full layer of material of thickness of 0.3 mm along z-axis. Standard element alive-dead approach of FEM, is employed in both thermal & structural steps to model the layer by layer process.[9] Only the elements of current and previously deposited layers are in active or alive state (contributing to conduction, stiffness, mass, etc.). Elements of the to-be-deposited layers are in dead state and do not contribute till they are turned alive. Each deposited layer undergoes a heat and cool cycle. The temperature in the molten filament deposited is approximated by an automatically computed heat-time for which the current layer is kept at its melting temperature. The cooldown-time, before the next layer is added is also controlled automatically by the ANSYS additive tool to ensure temperature gradients are similar in an actual build. Finally, we capture the full transient solution for the temperature using equation S1, that is mapped on the static structure for stress and deflection calculations.

Thermal boundary conditions imposed to solve equation S1 are: Base plate at constant temperature = 60 ˚C and the printed part has a heat transfer coefficient = 10 $W.m^{-2}.K^{-1}$ and exchanges heat with a chamber maintained at a constant temperature = 25 ˚C. Standard structural

finite element equations derived using the principle of virtual work are used for the static structural solution as given by equation S2.[6–8]

$$\left([K_e] + \left[K_e^f\right]\right)\{u\} - \{F_e^{th}\} = [M_e]\{\ddot{u}\} + \left\{F_e^{pr}\right\} + \{F_e^{nd}\} \qquad \text{(S2)}$$

where, $[K_e]$, $\left[K_e^f\right]$, $\{u\}$, $\{F_e^{th}\}$, $[M_e]$, $\left\{F_e^{pr}\right\}$, $\{F_e^{nd}\}$, are element stiffness matrix, element foundation stiffness matrix, primary displacement, element thermal load vector, element mass matrix, element pressure vector, element nodal load vector, respectively. Temperature dependent material constants like density and thermal expansion coefficient (CTE) are taken from the literature for HDPE.[10] The storage/tensile modulus for both waste-derived HDPE and f-HDPE are measured experimentally and are shown in Figure 2 of the main manuscript. These values are used in the simulations. Other material properties for polyethylene e.g. Poisson ratio, thermal conductivity and specific heat are taken from the literature and are listed in Table S1. We assume that the additives (0.4 wt. % DMDBS and 10% LLDPE) used in the f-HDPE blend do not change the thermal properties of the material. Therefore, we use same thermal properties for f-HDPE and for the neat waste-derived HDPE. However, the tensile modulus (E′) of the solid f-HDPE is lower compared to neat HDPE, as shown in Figure 2 (main manuscript). This effect is incorporated in our model. In the current model, the main contribution to the stresses developed is volume shrinkage as the polymer crystallizes. We consider that the melt state is stress-free, and stresses develop when the polymer shrinks as it cools and crystallizes. In this version of the FE model, we do not account for the effect of DMDBS on the melt modulus. We will incorporate this in future models.

Table S 3. List of parameters used in simulations

Parameter	value	Ref.
Specific heat, c_p ($Jkg^{-1}K^{-1}$)	1071	Gaur and Wunderlich[11]
Thermal Conductivity, k ($Wm^{-1}K^{-1}$)	0.52	Polymer Data handbook[10]
Heat of fusion, L, ($kJkg^{-1}$)	295.7	Polymer Data handbook[10]
Overall heat transfer coefficient, h, ($Wm^{-2}K^{-1}$)	10	Order of magnitude approximation

Base plate clamping is modelled by fixed displacements of the base plate. Appropriate dimensions of the glass base plate are used to place the build specimen of dimensions (length × breadth × height = 50 mm × 15 mm × 10 mm). FE layered mesh z-height is equal to 0.3 mm and other standard machine settings are used. **5070** linear hexahedral elements were used for the FE mesh for meshing both print substrate and the printed object. Two geometry variants are employed, one with direct build on base plate and another with a larger skirt (“brim”) of 1-layer height around the build specimen.

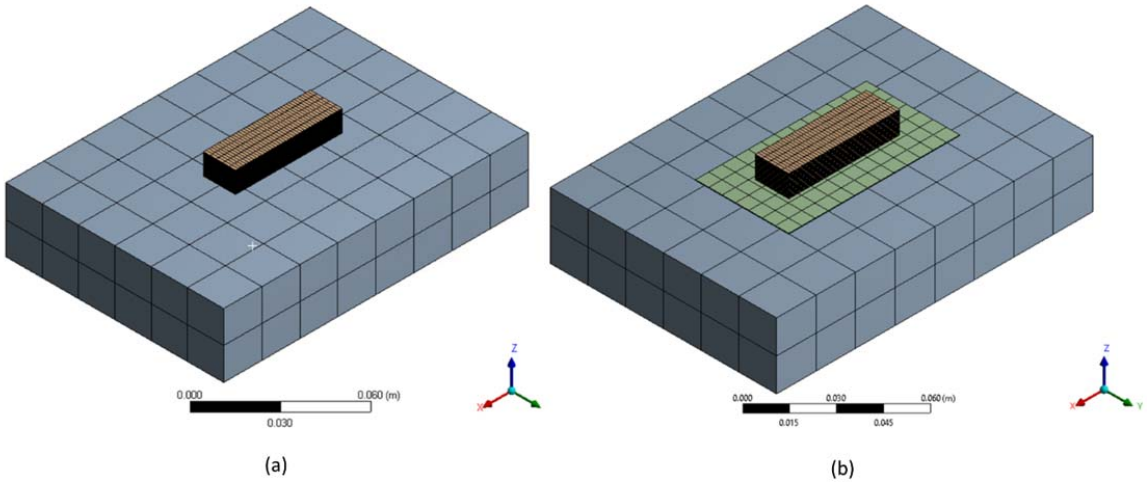

Figure S 10. Complete print object on the base plate and their meshing: (a) object without brim and (b) object with brim

We have considered two different height objects to compare the results with the experiments, e.g., 50 mm × 15 mm × 10 mm and 50 mm × 15 mm × 20 mm for the objects with brim. These objects are shown in Figure S7 and the results of contact stresses generated after cooling the object to room temperature are shown in Figure S8.

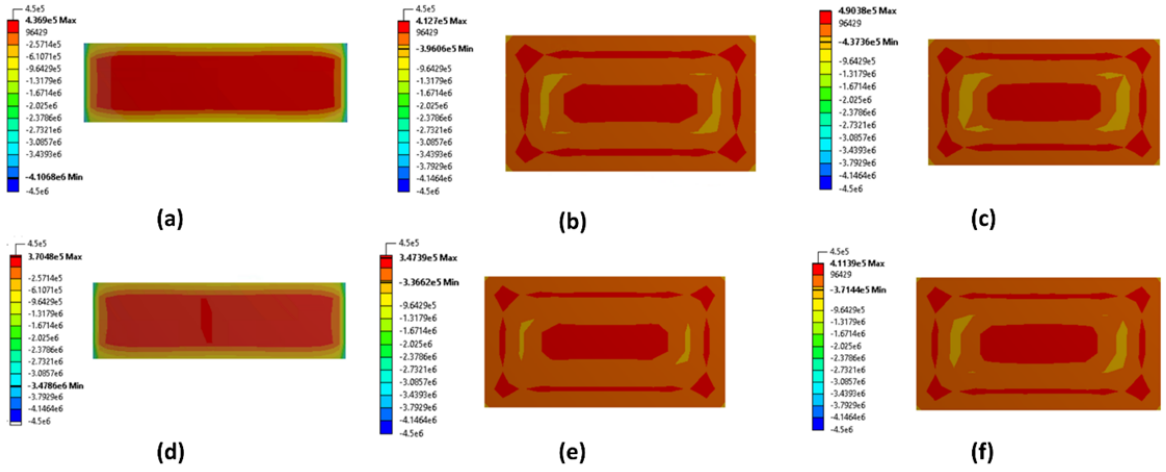

Figure S 11. Virtual contact stress generation at the base plate and object interface after printing. The negative stresses are tensile and positive stresses are compressive in nature. (a-c) shows contact stresses of neat recycled HDPE objects. (a) 10 mm object without brim, (b) 10 mm object with 13.5 mm brim and (c) 20 mm object with 13.5 mm brim. (d-f) shows contact stresses of f-HDPE objects. (d) 10 mm object without brim, (e) 10 mm object with 13.5 mm brim and (f) 20 mm object with 13.5 mm brim

References

(1) Weinhoffer, E. 3D printing a functional boat with post-consumer milk jugs https://makezine.com/2013/05/30/large-format-3d-printing/ (accessed Sep 26, 2019).

(2) Filgueira, D.; Holmen, S.; Melbø, J. K.; Moldes, D.; Echtermeyer, A. T.; Chinga-Carrasco, G. 3D Printable Filaments Made of Biobased Polyethylene Biocomposites. *Polymers (Basel).* **2018**, *10* (3).

(3) Peng, F.; Jiang, H.; Woods, A.; Joo, P.; Amis, E. J.; Zacharia, N. S.; Vogt, B. D. 3D Printing with Core–Shell Filaments Containing High or Low Density Polyethylene Shells. *ACS Appl. Polym. Mater.* **2019**, *1* (2), 275–285.

(4) Schirmeister, C. G.; Hees, T.; Licht, E. H.; Mülhaupt, R. 3D Printing of High Density Polyethylene by Fused Filament Fabrication. *Addit. Manuf.* **2019**, *28*, 152–159.

(5) Mead, D. W. Determination of Molecular Weight Distributions of Linear Flexible Polymers from Linear Viscoelastic Material Functions. *J. Rheol. (N. Y. N. Y).* **1994**, *38* (6), 1797–1827.

(6) Bathe, K.-J. *Finite Element Procedures*; Prentice-Hall: Englewood Cliffs, 1996.

(7) Cook, R. D. *Concepts and Applications of Finite Element Analysis*, 2nd ed.; John Wiley and Sons: New York, 1981.

(8) Bonet, J.; Wood, R. D. *Nonlinear Continuum Mechanics for Finite Element Analysis*; Cambridge University Press, 1997.

(9) Peng, H.; Go, D. B.; Billo, R.; Gong, S.; Shankar, M. R.; Gatrell, B. A.; Budzinski, J.; Ostiguy, P.; Attardo, R.; Tomonto, C.; et al. Part-Scale Model for Fast Prediction of Thermal Distortion in DMLS Additive Manufacturing; Part 2: A Quasi-Static Thermomechanical Model. In *Solid Freeform Fabrication 2016: Proceedings of the 27th Annual International Solid Freeform Fabrication 2016: Proceedings of the 2?th Annual International Solid Freeform Fabrication Symposium – An Additive Manufacturing Conference*; 2016; pp 382–397.

(10) Mark, J. E. *Polymer Data Handbook*, 2nd ed.; Mark, J. E., Ed.; Oxford University Press, 1999.

(11) Gaur, U.; Wunderlich, B. Heat Capacity and Other Thermodynamic Properties of Linear Macromolecules. V. Polystyrene. *J. Phys. Chem. Ref. Data* **1982**, *11* (2), 313–325.